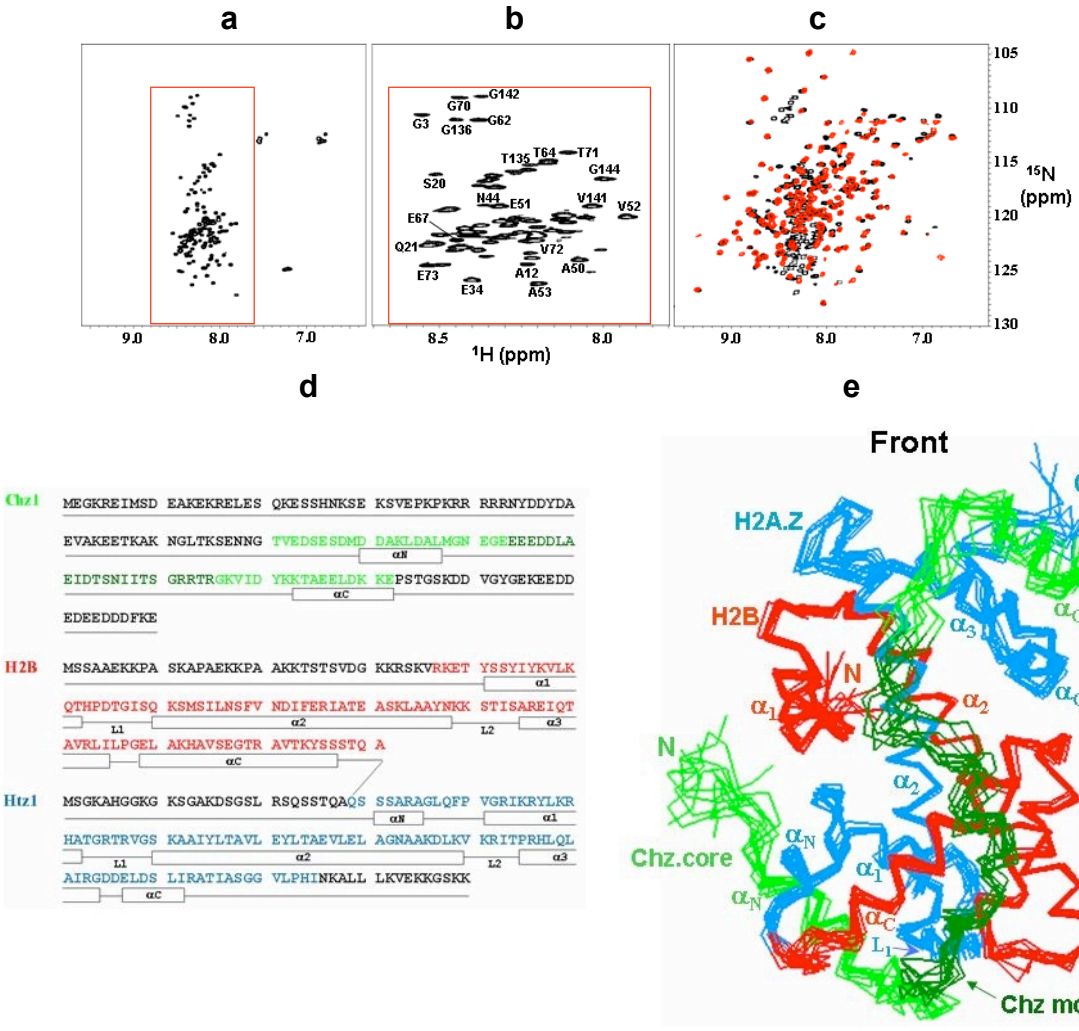
a
b
c
d
e
f
g
^{1}H (ppm)
^{15}N (ppm)
Chz1
H2B
Htz1
Front
H2A.Z
H2B
Chz.core
Chz motif
sH2B-H2A.Z
S29
A131
^{15}N-^{1}H S^{2}
1.0
0.8
0.6
0.4
<0.3

Supplementary Figure 1. Identification of unfolded regions in the Chz1-H2A.Z-H2B complex and structure and dynamics of Chz.core-sH2B_H2A.Z. (**a**) ^{1}H-^{15}N HSQC spectrum of Chz1. All backbone amide protons are in the narrow range from 7.6 ppm to 8.8 ppm (red frame), indicating that Chz1 alone is unstructured. (**b)** ^{1}H-^{15}N HSQC spectrum of Chz1-H2A.Z-H2B complex (~45 Kd) with [^{15}N, ^{13}C]-labeled Chz1 and non-labeled H2A.Z-H2B. The observed peaks are also in the same narrow range as in (**a)**, indicating they are in the unfolded regions of Chz1 in the Chz1-H2A.Z-H2B complex. The peaks that were assigned are labeled with single-letter amino acid codes followed by the residue numbers. (**c)** HSQC spectra of [^{15}N, ^{2}H]-labeled sH2B_H2A.Z (red) and [^{15}N, ^{2}H]-labeled full-length H2A.Z-H2B (black). The peaks that disappeared in the spectrum of sH2B_H2A.Z correspond to the strong peaks in the spectrum of the full-length H2A.Z-H2B. They are also in the narrow range of ^{1}H chemical shifts as in (**a)**, indicating that the deleted tails are unfolded in the full-length H2A.Z-H2B. The weak peaks in the two spectra are essentially identical, indicating that the reengineering has not perturbed the folded region. (**d)** The amino acid sequence of Chz1, H2A.Z and H2B. (**e)** Ca traces of 10 NMR structures of CZB superimposed on residues 7-132 in Chz.core, 47-131 in H2B, and 39-120 in H2A.Z. Chz.core, H2B, and H2A.Z are in green, red, and cyan, respectively. (**f**) Illustration of order parameters on the structure of the complex for sH2B_H2A.Z. (**g)** Illustration of order parameters on the structure of the complex for Chz.core. Structures of H2B (gray), H2A.Z (gray), and Chz.core (green) are represented with ribbons. The order parameters for measured residues are presented with colored balls.

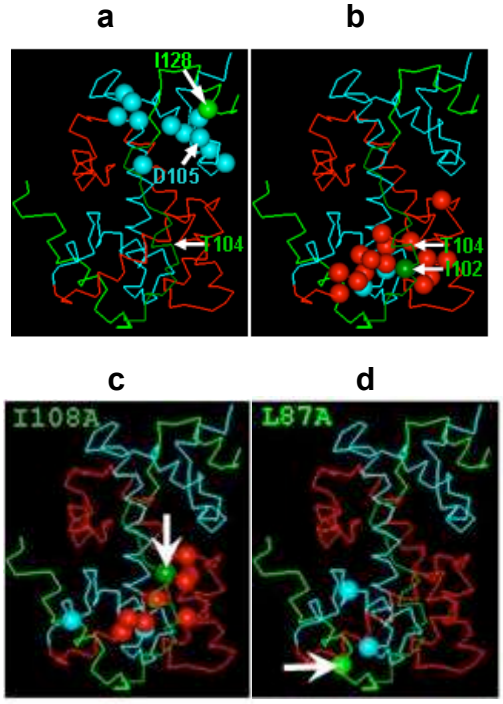

Supplementary Figure 2. Mutation-assisted identification of intermolecular NOEs. Residues with chemical shift changes of amide ^{1}H larger than 0.05 ppm or amide ^{15}N larger than 0.5 ppm in sH2B_H2A.Z were recorded as close neighbors of the mutation site. Residues in Chz.core, H2B, and H2A.Z are in green, red, and cyan, respectively. L128 $H_{\delta1}$ and T104 $H_{\gamma2}$ in Chz.core have similar chemical shifts that correspond to a cross-peak with D105 H_N of H2A.Z in the N^{15}-edited NOE spectrum. Therefore, this cross-peak may represent the NOE of H_N(H2A.Z D105)-$H_{\delta1}$(Chz.core L128) or H_N(H2A.Z D105)-$H_{\gamma2}$(Chz.core T104) or both. The L128A mutation in Chz.core affects the chemical shift of D105 H_N of H2A.Z (**a**), supporting that these two residues are close in distance. By contrast, the I102A mutation in Chz.core, which is at the neighbor site of T104 of Chz.core, has no effect on the chemical shifts of D105 of H2A.Z or its neighbor residues (**b**). Moreover, the I102A mutation affects the chemical shifts of the residues in the αC and α3 of H2B (red balls in **b**) that are far away from D105 of H2A.Z in the structure of sH2B_H2A.Z, indicating that Chz.core T104 is not close to H2A.Z D105 in space. Thus, the above mutation analyses unambiguously assign the NOE cross-peak to H_N(H2A.Z D105)-$H_{\delta1}$(Chz.core L128). (**c**) and (**d**) Additional two mutants as those shown in figure 1**b**. The residues that are affected by the mutations are shown in the following table.

Chz.core Mutations	[a]Residues in sH2B_H2A.Z (secondary structure) affected by mutations
M79A	41(α1), 43(α1), 60(α2)
A82G	34(αN), 41(α1), 53(L1), 54(L1), 60(α2), 62(α2)
L84A	40(α1), 126(αC), 39(L), 41(α1), 42(α1), 43(α1), 44(α1), 60(α2)

L87A	43(α2), 60(α2)
L99A	96(α3), 99(α3), 105(α3), 119(αC), 122(αC), 124(αC), 125(αC), 126(αC), 57(L1), 60(α2), 63(α2), 65(α2), 66(α2)
I102A	96(α3), 97(α3), 99(α3), 100(α3), 109(αC), 115(αC), 117(αC), 118(αC), 119(αC), 120(αC), 121(αC), 122(αC), 123(αC), 124(αC), 125(αC), 126(αC), 70(α2), 72(α2)
I107A	99(α3), 109(αC), 113(αC), 115(αC), 116(αC), 118(αC), 119(αC), 120(αC), 121(αC), 122(αC), 124(αC), 128(αC), 41(α1), 43(α1), 60(α2), 62(α2)
I108A	99(α3), 110(αC), 111(αC), 112(αC), 116(αC), 119(αC), 120(αC), 122(αC), 34(αN), 62(α2)
T114A	77(α2), 79(α2), 81(α2), 83(α2), 84(α2), 85(α2)
I119A	75(α2), 81(α2), 82(α2), 83(α2), 84(α2), 85(α2), 98(α3), 101(α3), 102(α3), 104(α3), 105(L), 109(αC)
L128A	76(α2), 81(α2), 83(α2), 84(α2), 85(α2), 101(α3), 102(α3), 104(α3), 105(L), 109(αC), 110(αC)

[a]Residues with chemical shift changes of amide ^{1}H larger than 0.05 ppm or amide ^{15}N larger than 0.5 ppm in sH2B_H2A.Z. Residues in Chz.core, H2B, and H2A.Z are in green, red, and cyan, respectively.

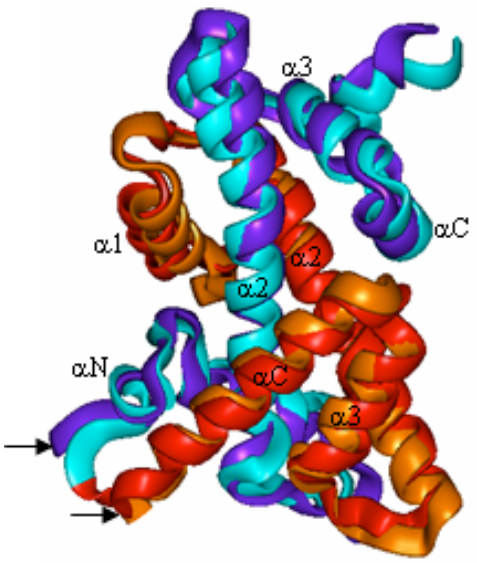

Supplementary Figure 3. Comparison of the structures of sH2B_H2A.Z in the CZB complex and H2B-H2A.Z in the nucleosome. The two structures are superimposed on their backbones and presented with ribbons. H2B and H2A.Z in sH2B_H2A.Z are in red and cyan, respectively; H2B and H2A.Z in the nucleosome are in brown and blue, respectively. The arrows indicate the C-terminus of H2B and N-terminus of H2A.Z in the structure of nucleosome. The similarity of the structure of sH2B_H2A.Z in the complex and the structure of H2B-H2A.Z further supports that single chain sH2B_H2A.Z did not change the histone structure. A single chain histone is made for two purposes: (1) to increase the stability of the complex so that the structure determination can be performed at higher temperature (35^{o}C) (High temperature is good for the sensitivity of NMR experiments); (2) to reduce the number of molecules to form the complex, which saves significant amount of time and money because expensive [^{15}N, ^{13}C, ^{2}H]-labelings of protein molecules are needed.

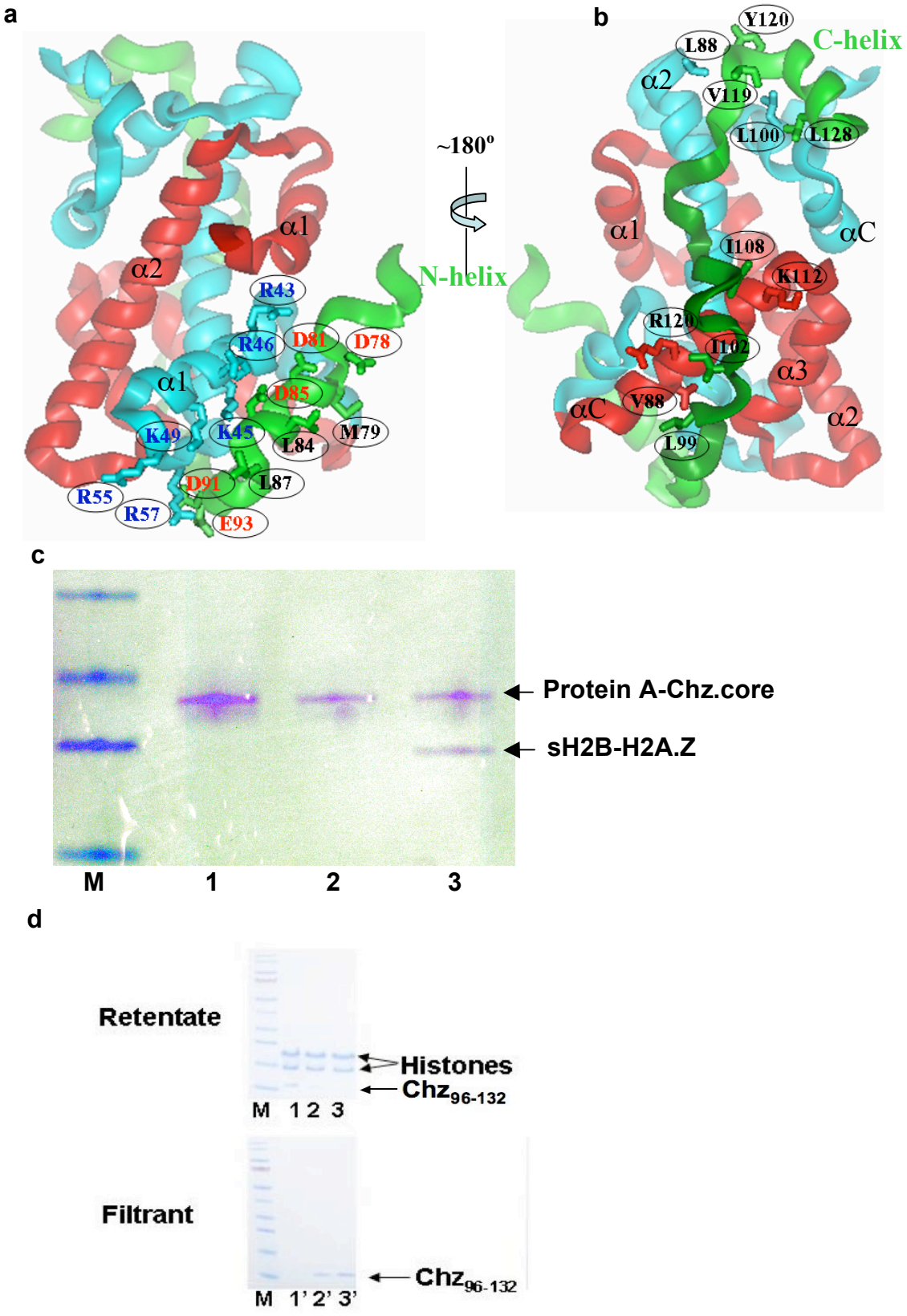
a
α1
α2
R43
R46
D81
D78
α1
D85
K49
K45
L84
M79
D91
L87
R55
R57
E93
~180°
N-helix
b
Y120
L88
C-helix
α2
V119
L100
L128
α1
αC
I108
K112
R120
I102
α3
αC
V88
α2
L99
c
Protein A-Chz.core
sH2B-H2A.Z
M
1
2
3
d
Retentate
Histones
Chz96-132
M 1 2 3
Filtrant
Chz96-132
M 1' 2' 3'

Supplementary Figure 4. Hydrophobic and electrostatic interactions between Chz.core and sH2B_H2A.Z. (**a)** Although there are three hydrophobic residues (M79, L84, and L87) in the N-helix of Chz.core, they don not form hydrophobic interactions with histones. (**b)**, Identifiable hydrophobic interactions between residue pairs, including $L99_{Chz.core}$-$V88_{H2B}$, $I102_{Chz.core}$-$R120_{H2B}$, and $I108_{Chz.core}$-$K112_{H2B}$, can be verified by the experimentally measured specific distance restraints. Possible hydrophobic interactions may also occur to residue pairs: $V119_{Chz.core}$-$L100_{H2A.Z}$, $Y120_{Chz.core}$-$L88_{H2A.Z}$, and $L128_{Chz.core}$-$G104_{H2A.Z}$. However, no observable specific distance restraints for these interactions could be identified and they only occur in some of the calculated structures. We note that the histone chaperone Asf1 forms complex with H3-H4 through broad interactions including electrostatic, hydrogen binding, and hydrophobic interactions, which is consistent with our emphasis that histone chaperones are not merely negatively charged molecules that are required to prevent nonproductive aggregation of histones with DNA phosphates. (**c**) Examination of the role of electrostatic interactions in the stablization of the CZB complex with different ionic strength (**Supplementary Methods**). M: molecular weight marker. Lane 1-3: Protein A-Chz.core-sH2B_H2A.Z complex was washed with 2M, 1M and 0.2 M NaCl solution, respectively. The upper arrow indicates the bands for protein A-Chz.core fusion protein. The lower arrow indicates the band for sH2B_H2A.Z. These results show that the CZB complex can be dissociated easily with the increase of ionic strength, indicating that electrostatic interactions play an important role for stabilizing the complex. (**d**) Stabilizing role of the electrostatic interactions between the positively charged residues in Chz.core and the acidic patch in histones. The experiments were done with mononuclesome and filtration method (see **Supplementary Methods**). Lane M: molecular weight marker. Lanes 1 and 1': wild type histones; Lanes 2 and 2': corresponding acidic patch residues (D105, E106 and E107 in H2A.Z and E109 in H2B) (Fig. 2c) were mutated to Q or N; Lanes 3 and 3': corresponding acidic patch residues (E71, D105, E106, and E107 in H2A and E109 in H2B) (Fig. 2c) were mutated to Q or N. These results showed that the Chz_{96-132} could bind to WT nucleosomes but not those with acidic patch mutations, suggesting that the electrostatic interactions play a critical role in stabilizing the complex.

Structural analysis also indicates that the electrostatic interactions derived from the structure should stabilize the complex. In the structure of the CZB complex, three regions in Chz.core form electrostatic interactions with H2A.Z-H2B: the N-helix (Fig. 2a), the negatively charged and the positively charged regions in the Chz motif (Fig. 2b). The N-helix (Fig. 2a) and the positively charged regions (Fig. 2b) in Chz.core must have used electrostatic interactions to stabilize the complex because no large hydrophobic residues exist at the interface between these two regions and the histones. In other words, if these electrostatic interactions did not play a stabilizing role, no other forces could account for the formation of the structures of these two regions in the complex. These results are fully consistent with the CZB structure in which a large number of charged residues form complementary electrostatic interactions between Chz.core and histones, whereas only few hydrophobic residues exist at their interface. They are also consistent with the fact that truncation of any of the large hydrophobic side chains in Chz.core did not disrupt the structure of the complex at 35^{o}C (Fig. 1b).

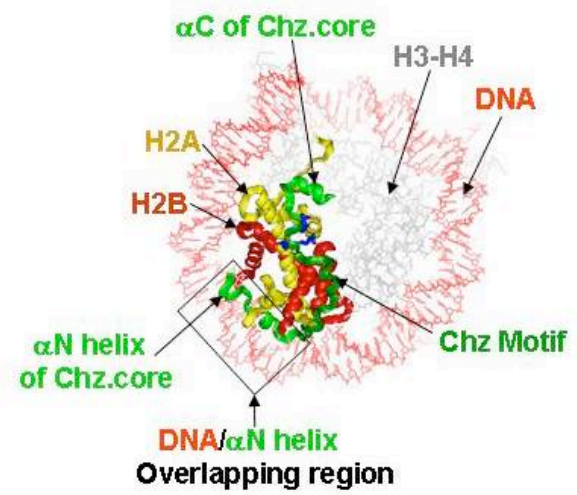

Supplementary Figure 5. Structural implications for the chaperone functions of Chz1. Position of Chz.core (green) after sH2B_H2A.Z (not shown) in the CZB complex is superimposed on H2B (yellow)-H2A (red) in the nucleosome. The N-helix of Chz.core occupies DNA-binding sites of H2A-H2B while the Chz motif and the C-helix sit on top of the exposed region of H2A-H2B in the nucleosome. The blue sticks in blue are Arg residues.

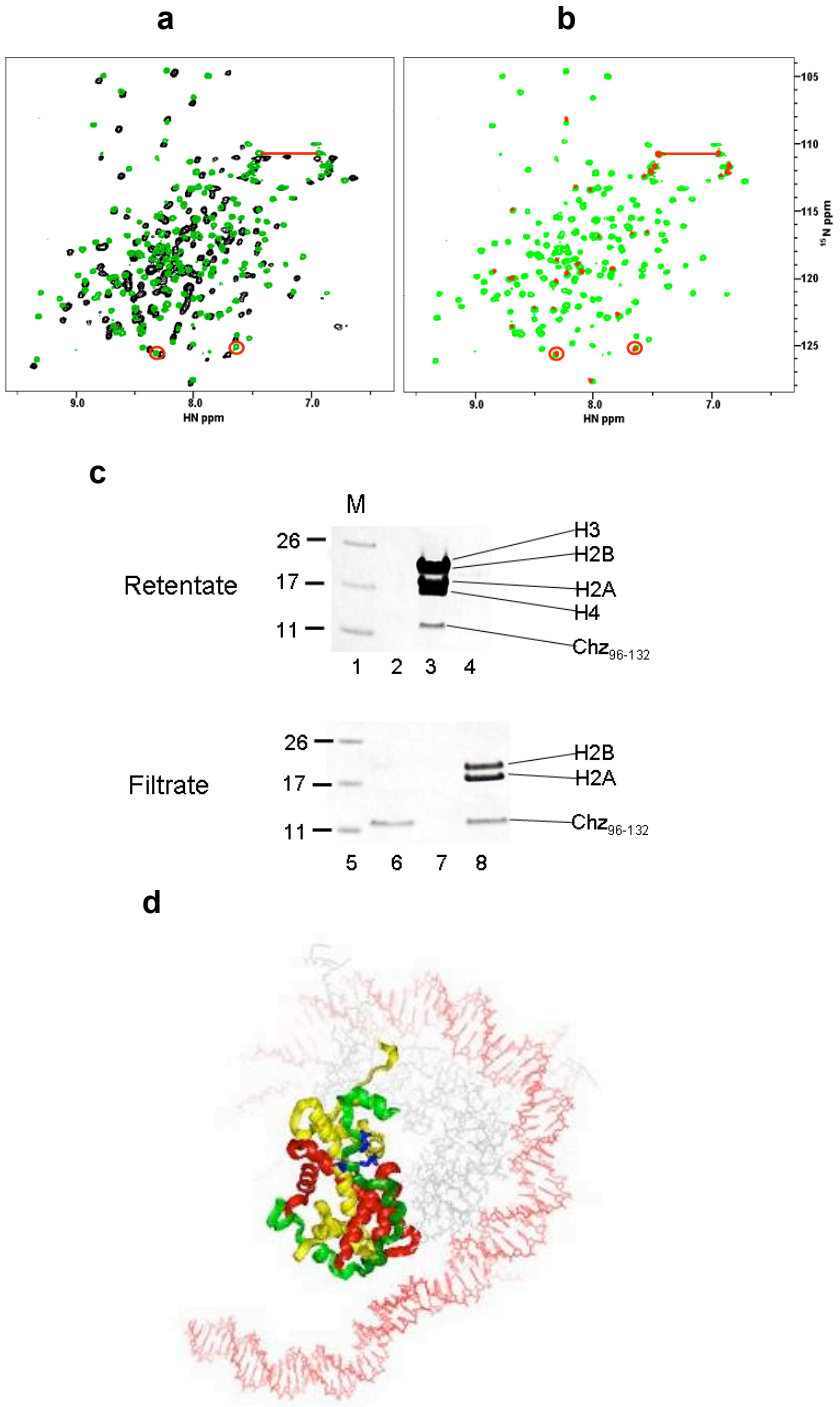

Supplementary Figure 6. Binding of Chz_{96-132} to sH2B_H2A.Z and mononucleosomes and its implications for potential H2A-H2B eviction. (**a)** Overlay of the ^{1}H-^{15}N HSQC spectra of non-labeled Chz_{96-132} complexed with ^{15}N-labeled sH2B_H2A.Z at 280 μM (green) and ^{15}N-labeled sH2B_H2A.Z alone (black). The change of peak positions in the two spectra indicates that Chz_{96-132} binds to sH2B_H2A.Z. (**b**) Overlay of the ^{1}H-^{15}N HSQC spectra of non-labeled Chz_{96-132} complexed with ^{15}N-labeled sH2B_H2A.Z at 280 μM (green) and 10 μM (red). The observable peaks at 10 μM overlap with the corresponding peaks at 280 μM. The disappearance of many peaks is likely due to the

dissociation/association between sH2B_H2A.Z and Chz_{96-132} on the time scale that causes broadening of these peaks. The red circles and lines are used to emphasize that the peaks marked by them must arise from the complex. (**c)** SDS page gel detection for the binding between Chz_{96-132} and H2A-H2B/mononucleosome at ~3 μM. Lanes 1 and 5: molecular weight markers; Lanes 2, 3, and 4: proteins retained in the microcons after the filtrations of Chz_{96-132}, NCP-Chz_{96-132} , and Chz_{96-132}-H2A-H2B, respectively. Lanes 6, 7, and 8: flow-through of Chz_{96-132} , NCP-Chz_{96-132} , and Chz_{96-132}-H2A-H2B, respectively. Note that no H2A-H2B eviction by Chz1 alone at a molar ratio of 1:1 between Chz1 and nucleosome was observed (data not shown). (**d)**, Coupled folding and binding of Chz.core to H2A-H2B after DNA is presumably locally dissociated from H2A-H2B in the nucleosome by SWR1. The blue sticks in blue are Arg residues. The established *in vitro* H2A.Z exchange assay under limiting amount of SWR1 showed that H2A.Z could be incorporated into chromatin in the presence of Chz1 (at a level similar to histone) and also in its absence (see Figure 5C of Luk et al. Mol Cell 25: p363, 2007). The replacement was somewhat less efficient in the absence of Chz1. Although this result appears to be consistent with the potential role of Chz1 on H2A-H2B eviction, we do not consider it a conclusive test for the above model because loss of histone dimers due to precipitation in the absence of chaperone cannot be easily controlled. Moreover, even in the absence of any precipitation, such test would not allow one to make definitive conclusions about the eviction process because the outcome of the experiment (controlled by the thermodynamics) does not necessarily reflect the eviction process (kinetics). An alternative approach that can monitor the eviction process such as the time-dependent photo cross-linking method is needed to test the model conclusively.

Supplementary Table 1. NMR and refinement statistics for the CZB structures.

	Chz.core-sH2B_H2A.Z
NMR distance and dihedral constraints	
Distance constraints	
Total NOE	4280
Intra-residue	765
Inter-residue	3515
Sequential ($\|i-j\|=1$)	1234
Medium-range ($\|i-j\|<4$)	1201
Long-range ($\|i-j\|>5$)	1008
Intermolecular	79
Hydrogen bonds	196
Total dihedral angle restraints	
ϕ	123
ψ	122
$^{3}J_{HN\text{-}Ca}$	111
Structure statistics	
Violations (mean ± s.d.)	
Distance constraints (Å)	0.0401 ± 0.002
Dihedral angle constraints (º)	0.161 ± 0.02
Max. dihedral angle violation (º)	3.55
Max. distance constraint violation (Å)	0.31
Deviations from idealized geometry	
Bond lengths (Å)	0.0049 ± 0.0001
Bond angles (º)	0.60 ± 0.03
Impropers (º)	0.4 ± 0.2
Average pairwise r.m.s. deviation (Å)	
Heavy	1.45
Backbone	0.87

Pairwise r.m.s. deviation was calculated among 20 refined structures.

Supplementary Methods

Chemical shift assignments, measurements of NOEs, and structure calculations

Chemical shifts (^{1}H, ^{15}N, and ^{13}C) were assigned by performing triple-resonance experiments. Intermolecular NOEs were obtained from ^{15}N-edited NOESY experiments on [^{15}N, ^{2}H]-labeled sH2B_H2A.Z complexed with non-labeled Chz.core and [^{15}N, ^{2}H]-labeled Chz.core complexed with non-labeled sH2B_H2A.Z. Samples and pulse programs are shown in the following table.

No.	a: Htz1-H2B b: sH2B-Htz1	c: Chz1 d: Chz.core	NMR experiments	Notes
1	Non-labeled[a]	^{15}N[c]	^{15}N HSQC	Assignments of unfolded residues in Chz1
2	Non-labeled[a]	(^{15}N, ^{13}C)[c]	HNCACB CBCACONH	Assignment of unfolded residues in Chz1
3	(^{15}N, ^{13}C, ^{2}H)[b]	Non-labeled[d]	TRHNCACB, TRHNCOCACB, TRHNCO TRHNCOCA, TRHNCA, CCCONH	Backbone assignments of sH2B-Htz1
4	(^{15}N, ^{13}C, 70% or 30% ^{2}H)[b]	(^{15}N, ^{13}C, ^{2}H)[d]	HCCCONH, HCCH-TOCSY ^{15}N-edited TOCSY	Histones side chain assignments
5	^{15}N[b]	^{15}N[d]	^{15}N-edited NOESY	NOE determination
6	(^{15}N, 75%^{2}H)[b]	(^{15}N, 75% ^{2}H)[d]	^{15}N-edited NOESY	NOE determination
7	^{15}N[b]	(^{15}N, ^{13}C, ^{2}H)[d]	TRHNCACB, TRHNCOCACB, TRHNCO TRHNCOCA, TRHNCA, CCCONH	Backbone assignments of Chz.core
8	(^{15}N, 75% ^{2}H)[b]	(^{15}N, 75% ^{2}H)[d]	NNOE, HNHA ^{15}N-edited TOCSY	Assignments and NOE determination
9	(^{15}N, ^{13}C, 75% ^{2}H)	(^{15}N, ^{13}C, 75% ^{2}H)	HCCCONH HBHACONH	Side chain assignment
10	(^{15}N, 75%^{2}H)[b]	(^{15}N, 75%^{2}H)[d]	HCCH TOCSY C-NOESYHSQC	Assignments
11	(99.9% ^{2}H or ^{15}N, 75% ^{2}H)[b]	(^{15}N, 75% ^{2}H or 99.9% ^{2}H)[d]	N-NOESYHSQC (intra-protein)	NOE determination
12	(^{15}N, 99.9%^{2}H or 99.9% ^{2}H)[b]	(99.9% ^{2}H or ^{15}N, 99.9%^{2}H)[d]	N-NOESYHSQC (inter-protein)	NOE determination

13	(^{13}C, 75% or 25% ^{2}H)[b]	(99.9% ^{2}H)[d]	HCCH TOCSY C-NOESYHSQC	Assignment and NOE determination
14	(99.9% ^{2}H)[b]	(^{13}C, 75% or 25% ^{2}H)[d]	HCCH TOCSY C-NOESYHSQC	Assignment and NOE determination
15	(^{13}C, 35%2H)[b]	(99.9% ^{2}H)[d]	^{13}C NOESYHSQC HCCHTOCSY	Assignments and NOE determination
16	(75% ^{2}H)[b]	(75% ^{2}H)[d]	NOESY	Assignment and NOE determination
17	(^{15}N, 35% ^{2}H)[b]	(99.9% ^{2}H)[d]	NNOE, HNHA	Assignments
18	(^{15}N, ^{13}C, 75% ^{2}H, or 99.9% ^{2}H)[b]	(99.9% ^{2}H or ^{15}N, ^{13}C, 75% ^{2}H)[d]	HNCANNH	Assignment confirmation

NMR data were processed with NMRPipe/NMRDraw[1], and analyzed with NMRVIEW[2]. The NOE-derived restraints were subdivided into four classes, strong (1.8–2.7 Å), medium (1.8–3.3 Å), weak (1.8–5.0 Å), and very weak (1.8–6.0 Å), by comparison with NOEs of protons separated by known distances[3]. An extra 0.5 Å was added to the upper distance limit for methyl protons. An extra 0.2 Å was added to the upper distance limit for NH protons if the NOEs were in the strong and medium classes. Backbone dihedral angle restraints (φ and ψ angles) were obtained from analysis of $^{1}H_{\alpha}$, HN, $^{13}C_{\alpha}$, $^{13}C_{\beta}$, ^{13}CO, and ^{15}N chemical shifts by using the program TALOS[4]. Hydrogen bonds were identified on the basis of exchange rates of amide protons with $^{2}H_2O$. Amide protons that did not exchange significantly after the CZB complex was dissolved in $^{2}H_2O$ for ~12 hours at 35°C and pH 6.0 were considered to form hydrogen bonds in the complex. Two constants per hydrogen bond ($d_{NH-O} \leq 2.2$ Å and $d_{N-O} \leq 3.2$ Å) were added in the final structure calculation after initial NOE-derived structures were obtained. Structures were calculated using conjoined rigid body/torsion angle simulated annealing with the program Xplor-NIH. The quality of the structures was analyzed by using the program PROCHECK_NMR[5]. Ramachandran plot statistics: most favored, 68.3%; allowed, 18.2%; generously allowed, 6.8%; disallowed, 1.5%.

Dynamics of the CZB complex

[^{15}N, ^{2}H]-labeled CZB at ~1 mM was used for the dynamics studies of the complex at pH 6.0 and 35°C with a buffer solution containing 25 mM MES, 0.2 mM NaCl, 1 mM EDTA, and 10 % (v/v) D_2O. Nitrogen R_1 and $R_{1\rho}$ relaxation rates along with steady-state ^{15}N-{^{1}H} NOE values were obtained for the backbone amides at static magnetic field strengths of 18.8 T (R_1, $R_{1\rho}$, NOE); 14.1 T (R_1, NOE) and 11.7 T (R_1). Relaxation delays in the range from 0.01 to 1.4 sec and from 0.002 to 0.1 sec were used to monitor the R_1 and $R_{1\rho}$ rates, respectively. The CW field strength applied during the spin-lock period in the $R_{1\rho}$ experiment was 2.0 kHz. The ^{15}N-{^{1}H} NOEs were determined from two spectra, with and without proton pre-saturation. The spectrum with pre-saturation was recorded with a pre-scan delay of 9 seconds followed by 6 seconds of proton saturation, while the spectrum without proton pre-saturation was recorded with a 15-second pre-scan delay.

An exchange-free measure of the transverse nitrogen relaxation, R_{dd}, was derived from the four relaxation rates $R_{1\rho}(2H'_zN_z)$, $R_{1\rho}(2H_zN'_z)$, $R_{1\rho^2}(2H'_zN'_z)$, and $R_1(2H_zN_z)$ that were measured at 18.8 T using pulse schemes described recently[1]. Relaxation delays in the range from 2 to 25 msec were used for all experiments (same delays used for each rate measurement), along with ^{1}H and ^{15}N continuous wave CW spin-lock field strengths that varied between 11.0 kHz (^{1}H) and 2.0 kHz (^{15}N). A total of 10 2D data sets was recorded for each relaxation rate determination.

Data sets were processed with the NMRPipe program and analyzed with Sparky (Goddard, T.D. & Kneller, D.G., UCSF). Signal intensities were determined using the program FuDA (Kristensen, S. M. and Hansen, D. F., smk@kiku.dk, available upon request) by fitting a mixed Gaussian/Lorentzian lineshape to each correlation and assuming a common line-shape for a given cross-peak during a relaxation series (*i.e.* line-shape and peak positions are independent of T_{relax}). Relaxation rates were determined by fitting a single exponential decay function [$I(T_{relax}) = A\exp(-R\ T_{relax})$] to the measured intensity *vs*. T_{relax} profile. The exchange-free measure of the transverse nitrogen relaxation, R_{dd}, along with values for ^{15}N R_1, ^{1}H-^{15}N NOE and the NMR structure of the CZB were used to derive the generalized order parameters of the backbone, $\boldsymbol{S}^2$ and the diffusion parameters via the program ModelFree 4.16 (Palmer, A. G. III., agp@columbia.edu).

Binding of Chz$_{96\text{-}132}$ to sH2B_H2A.Z and mononucleosome

[^{15}N, ^{2}H]-labeled sH2B_H2A.Z complexed with non-labeled Chz$_{96\text{-}132}$ was made at 280 μM and subsequently diluted to 10 μM. The nucleosome core particle (NCP) was reconstituted using recombinant histones from *Drosophila melanogaste*r and a 146 bp palindromic DNA fragment derived from human α satellite DNA[6]. *Drosophila* nucleosome was used because it can be reconstituted with higher yield and the amino acid sequences of H2A-H2B in the exposed region in the nucleosome are essentially identical between *Drosophila* and *yeast*. The reconstituted NCP was purified by DEAE-5PW HPLC column (TOSOH) and subjected to heat-shifting to localize the histone octamer to the center of DNA. NCP and Chz$_{96\text{-}132}$ peptide were mixed at an equal molar ratio (measured by optical density at 280 nm) in 25 mM MES buffer solution (pH 6.0) and kept on ice for 30 minutes. The samples (200 μl, ~3.5 μM) were concentrated to about 30 μl with Microcon 100 (Amicon) with a cut-off size of 100 kDa. They were diluted to 210 μl by adding 180 μl buffer and concentrated again. This procedure was repeated three times. The retentate and filtrate were collected, dried with a rotary evaporator and analyzed by SDS-PAGE (4 – 12 %).

Effect of ionic strength on the binding between Chz.core and sH2B_H2A.Z

IgG-Sepharose resin 10 ul was washed extensively with wash buffer (25mM HEPES-KOH, 1mM EDTA, 10% glycerol, 0.01% NP-40, 0.2M NaCl, pH7.6). Protein A-Chz core fusion protein (final concentration is 2.5 μM) was incubated with IgG-Sepharose resin for 1 hr at 25 ^{o}C. The unbound proteins were removed by centrifuge at 2000X*g* for 1 min and the resins were washed with 1 ml wash buffer for 3 times. 200 μM sH2A.Z-H2B then was added with the final concentration of 0.3 μM and incubated with the resins for 1 hr at 25 ^{o}C. After removing supernatant, 1 ml wash buffers with different

concentration of NaCl were applied to wash the resins for 5 times. Resins were spun down and subsequently resuspended in 30 μl SDS loading buffer (22.5ul 1% SDS, 8M Urea, 10mM DTT, 7.5 μl dye). 1 μl of each sample was applied to SDS-PAGE. The gel was stained with Coomassie Blue.

Supplementary References

1. Delaglio, F. *et al.* NMRPipe: a multidimensional spectral processing system based on UNIX pipes. *J. Biomol. NMR* **6**, 277-293 (1995).

2. Johnson, B. A. & Blevins, R. A. NMR View: A computer program for the visualization and analysis of NMR data. *J. Biomol. NMR* **4**, 603-614 (1994).

3. Nguyen, B. D. *et al.* Solution Structure of the Carboxyl-Terminal Domain of RAP74 and NMR Characterization of the FCP1-Binding Sites of RAP74 and Human TFIIB. *Biochemistry* **42**, 1460-1469 (2003).

4. Cornilescu, G., Delaglio, F. & Bax, A. Protein backbone angle restraints from searching a database for chemical shift and sequence homology. *J. Biomol. NMR* **13**, 289-302 (1999).

5. Laskowski, R. A. *et al.* AQUA and PROCHECK-NMR: Programs for checking the quality of protein structures solved by NMR. *J. Biomol. NMR* **8**, 477-486 (1996).

6. Dyer, P. N. *et al.* Reconstitution of nucleosome core particles from recombinant histones and DNA. *Methods Enzymol.* **375**, 23-44 (2004).